

# Radio detection of air showers with LOFAR and AERA

Jörg R. HÖRANDEL<sup>1,2</sup> on behalf of the LOFAR key science project Cosmic Rays and the Pierre Auger Collaboration

<sup>1</sup>*Radboud University Nijmegen, Department of Astrophysics, IMAPP, P.O. Box 9010, 6500 GL Nijmegen, The Netherlands, <http://particle.astro.ru.nl>*

<sup>2</sup>*Nikhef*

*E-mail: [j.horandel@astro.ru.nl](mailto:j.horandel@astro.ru.nl)*

**KEYWORDS:** UHECR 2014, cosmic rays, air showers, radio emission, radio detection

## 1. Introduction

To understand the origin of high-energy cosmic rays is one of the open key questions in astroparticle physics [1, 2]. An inspiring article, published in 2003 [3] heralded the renaissance of radio detection of extensive air showers with the ultimate goal to measure the properties of cosmic rays with this technique and the pioneer experiments LOPES [4] and CODALEMA [5] were initiated. The big success of these pathfinders stimulated further investigations of the radio emission of air showers on larger scales, with installations such as Tunka-Rex [6], AERA (Auger Engineering Radio Array) at the Pierre Auger Observatory, and the LOFAR radio telescope. Significant progress has been achieved in the last decade [7] and we now understand the emission processes of the radio waves in the atmosphere. Most of the emission is due to the interaction of the shower with the magnetic field of the Earth, which leads to a transverse current in the shower. In addition to this emission, the overabundance of electrons in the shower that are collected from atmospheric molecules leads to a current in the direction of the shower.

## 2. Radio Air-Shower Detectors

Two modern radio detectors for extensive air showers are the LOFAR radio telescope (in particular, its dense core in the Netherlands) and AERA at the Pierre Auger Observatory in Argentina. The layout of the two set-ups is drawn to scale in Fig. 1.

**LOFAR radio telescope** The LOFAR key science project Cosmic Rays represents one of the six scientific key objectives of LOFAR [8, 9]. LOFAR is a digital radio telescope. Its antennas are spread over several European countries and are used together for interferometric radio observations in the frequency range of 10 – 240 MHz. The density of antennas increases towards the center of LOFAR, which is located in the Netherlands. Here, about 2400 antennas are clustered on an area of roughly 10 km<sup>2</sup>. This high density of antennas makes LOFAR the perfect tool to study features of the radio emission created by extensive air showers. Air-shower measurements are conducted based on a trigger received from an array of scintillators (LORA) [10, 11], which results in a read-out of the ring buffers that store the raw voltage traces per antenna for up to 5 s. LOFAR comprises two types of antennas, recording radio emission in low-frequency band from 10 to 90 MHz and also in the high-frequency band (110 – 240 MHz).

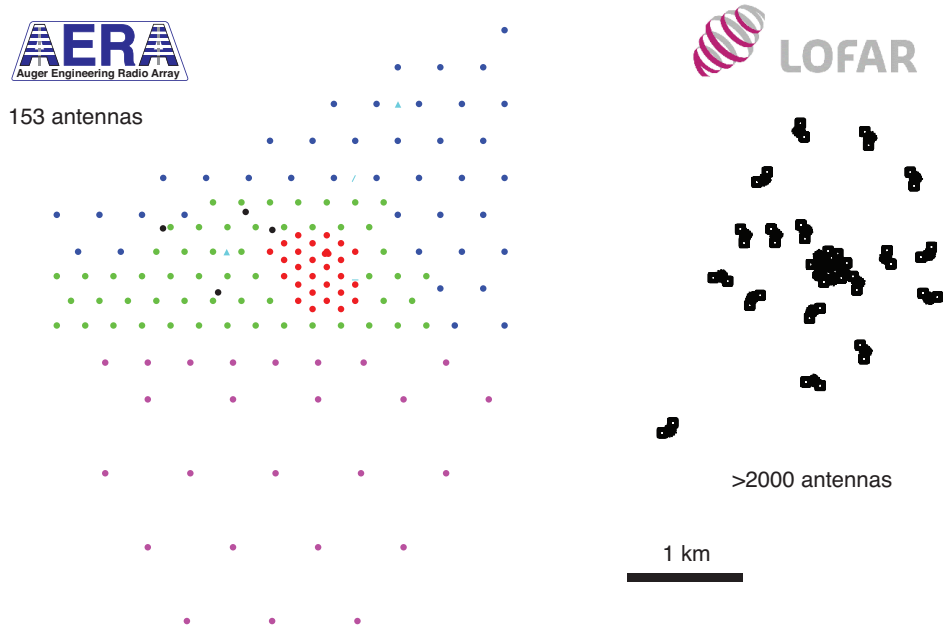


**Fig. 1.** Layout of AERA at the Pierre Auger Observatory and the dense core of LOFAR – drawn to scale.

**AERA at the Pierre Auger Observatory** AERA is a radio extension of the Pierre Auger Observatory. The Observatory is a 3000-km<sup>2</sup> hybrid cosmic-ray air-shower detector in Argentina [12, 13], with an array of 1660 water-Čerenkov detectors and 27 fluorescence telescopes at four locations on the periphery [14]. The area near the Coihueco fluorescence detector contains a number of low-energy enhancements, including AERA. AERA is located in a region with a higher density of water-Čerenkov detectors (on a 750 m grid) and within the field of view of HEAT [15], allowing for the calibration of the radio signal using super-hybrid air-shower measurements, i.e., recording simultaneously the fluorescence light, the particles at the ground, and the radio emission from extensive air showers.

Since March 2015 AERA consists of 153 autonomous radio-detection stations, distributed with different spacings, ranging from 150 m in the dense core up to 750 m, covering an area of about 17 km<sup>2</sup>. Different types of antennas are used, including logarithmic periodic dipoles and active bowtie antennas (named "Butterfly antennas" [16]) covering the frequency range from 30 to 80 MHz [17, 18].

### 3. Precision measurement of the radio emission in air showers

LOFAR combines a high antenna density and a fast sampling of the measured voltage traces in each antenna. This yields very detailed information for each measured air shower and the properties of the radio emission have been measured with high precision. At the Pierre Auger Observatory air showers are measured simultaneously with various detector systems: radio detectors, fluorescence light telescopes, water-Čerenkov detectors, and underground muon detectors. This unique combination yields complementary information about the showers and allows to investigate correlations between the various shower components. Some important aspects of radio emission in air showers are reviewed in the following. We focus on radio emission in the frequency range 30 – 80 MHz, only one result (Fig. 3 *right*) deals with higher frequencies.

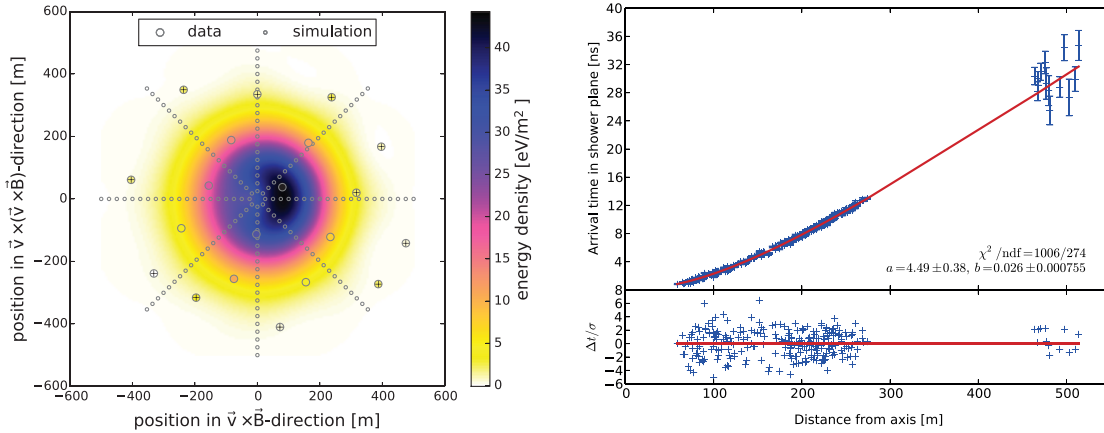


**Fig. 2.** *Left:* Footprint of an air shower measured with AERA at the Pierre Auger Observatory, the boxes representing the radio-detector stations. The colored background represents predictions of the radio signal according to simulations [19]. *Right:* The arrival time of the signals, relative to a plane as a function to the distance to the shower axis as measured with LOFAR. The lower right graph illustrates the arrival time differences with respect to a fit (hyperboloid) [20].

**Lateral distribution function of the radio signals** The footprint of the radio emission recorded at ground level is not rotationally symmetric [19, 21, 22], such as, e.g., the particle content of a shower, see Fig. 2 (*left*). Radio emission is generated through interactions with the Earth magnetic field, which yields a bean-shaped footprint on the ground. The correct reference system is in the shower plane (perpendicular to the shower axis), with one coordinate axis along the  $\vec{v} \times \vec{B}$  direction and the second axis along the  $\vec{v}$  ( $\vec{v} \times \vec{B}$ ) direction. Here  $\vec{v}$  is the propagation velocity vector of the shower (parallel to the shower axis) and  $\vec{B}$  represents the direction and strength of the Earth magnetic field. The measured power in the frequency range 30 – 80 MHz is plotted as a function of the distance to the shower axis in Fig. 3 (*left*). For example at a distance of 200 m from the shower axis, ambiguities are visible in this one-dimensional projection: the recorded signal strength is a function of the azimuth angle, which results in the visible structure. Historically, the lateral distribution of the radio signal on the ground has often been parameterized with a simple exponential function (e.g., [23]). However, the LOFAR measurements suggest that the radio emission should be parameterized by a more complex expression: a two-dimensional Gaussian function is used to describe the approximately exponential fall-off at large distances from the shower axis. A second (smaller) two-dimensional Gaussian function is subtracted from the first one to describe the ring structure of the signal close to the shower axis. To reproduce the observed bean shape, the centers of both Gaussian functions are slightly offset. The power at position  $(x', y')$  in the shower plane (perpendicular to the shower axis) is described as

$$P(x', y') = A_+ \exp\left(-\frac{(x' - X_+)^2 + (y' - Y_+)^2}{\sigma_+^2}\right) - A_- \exp\left(-\frac{(x' - X_-)^2 + (y' - Y_-)^2}{\sigma_-^2}\right), \quad (1)$$

Where the parameters are the scaling factors  $A_+$  and  $A_-$  (where in general  $A_+ \gg A_-$ ), the width of the Gaussian functions  $\sigma_+$  and  $\sigma_-$ , and the centers of the two-dimensional Gaussian distributions  $(X_+, Y_+)$  and  $(X_-, Y_-)$ , respectively.

**First quantitative measurements in the frequency range 120-240 MHz** Radio emission from extensive air showers has also been recorded with the LOFAR high-band antennas in the 200 MHz frequency domain [24]. The measured power is depicted in Fig. 3 (*right*) as a function of the distance to the shower axis. A clear maximum is visible at distances around 120 m in this one-dimensional projection, indicating a clear (Čerenkov) ring structure. Such rings are predicted from theory: rela-

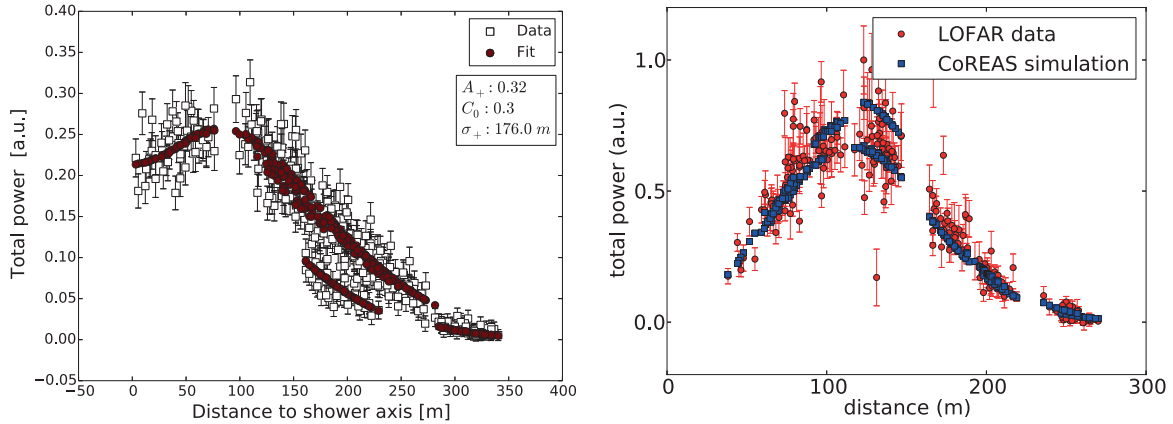


**Fig. 3.** Total power measured in an air shower as a function of the distance to the shower axis (in the shower plane) as measured by LOFAR in the frequency range 30 – 80 MHz (*left*) [22] and 110 – 190 MHz (*right*) [24].

tivistic time compression effects lead to a ring of amplified emission, which starts to dominate the emission pattern for frequencies above  $\sim 100$  MHz. The LOFAR data clearly confirm the importance to include the index of refraction of air as a function of height into calculations of the radio emission.

**Shape of the shower front** The precise shape of the radio wavefront is a long-standing issue. In the literature different scenarios have been discussed: a spherical, conical, or hyperbolic shape (e.g. [25]). The LOFAR findings clearly indicate that a hyperboloid is the best way to describe the shape of the measured wavefront [20]. A hyperboloid asymptotically reaches a conical shape at large distances from the shower axis and can be approximated as a sphere close to the shower axis. A measured wavefront of a shower registered with LOFAR is shown in Fig. 2 (*right*). The time difference relative to a plane is plotted as a function of distance to the shower axis. The line indicates a fit of a hyperboloid to the measured data. The lower part of the graph shows the time differences of the individual antennas with respect to the fit function.

**Polarization of the radio signal** The radio emission in extensive air showers originates from different processes. The dominant mechanism is of geomagnetic origin [4, 26]. Electrons and positrons in the shower are accelerated in opposite directions by the Lorentz force exerted by the magnetic field of the Earth. The generated radio emission is linearly polarized in the direction of the Lorentz force ( $\vec{v} \times \vec{B}$ ), where  $\vec{v}$  is the propagation velocity vector of the shower (parallel to the shower axis) and  $\vec{B}$  represents the direction and strength of the Earth magnetic field. A secondary contribution to the radio emission results from the excess of electrons at the front of the shower (Askaryan effect) [27, 28]. This excess is built up from electrons that are knocked out of atmospheric molecules by interactions with shower particles and by a net depletion of positrons due to annihilation. This charge excess contribution is radially polarized, pointing towards the shower axis. The resulting emission measured at the ground is the sum of both components. Interference between these components may be constructive or destructive, depending on the position of the observer/antenna relative to the shower. The emission is strongly beamed in the forward direction due to the relativistic velocities of the particles. Additionally, the emission propagates through the atmosphere, which has a non-unity index of refraction that changes with height. This gives rise to relativistic time-compression effects, most prominently resulting in a ring of amplified emission around the Čerenkov angle, see Fig. 3. By precisely measuring the polarization direction of the electric field at each antenna position, the ratio  $a$  between the contributions from the Askaryan effect and the geomagnetic emission is measured. The resulting ratios as measured at the Auger Observatory for individual air showers are shown in Fig. 4 (*left*) [29]. An average value of  $a = 14\% \pm 2\%$  is obtained. At LOFAR the ratio  $a$  has been measured as a function of the distance to the shower axis for showers with different zenith angles, as depicted in Fig. 4 (*right*)

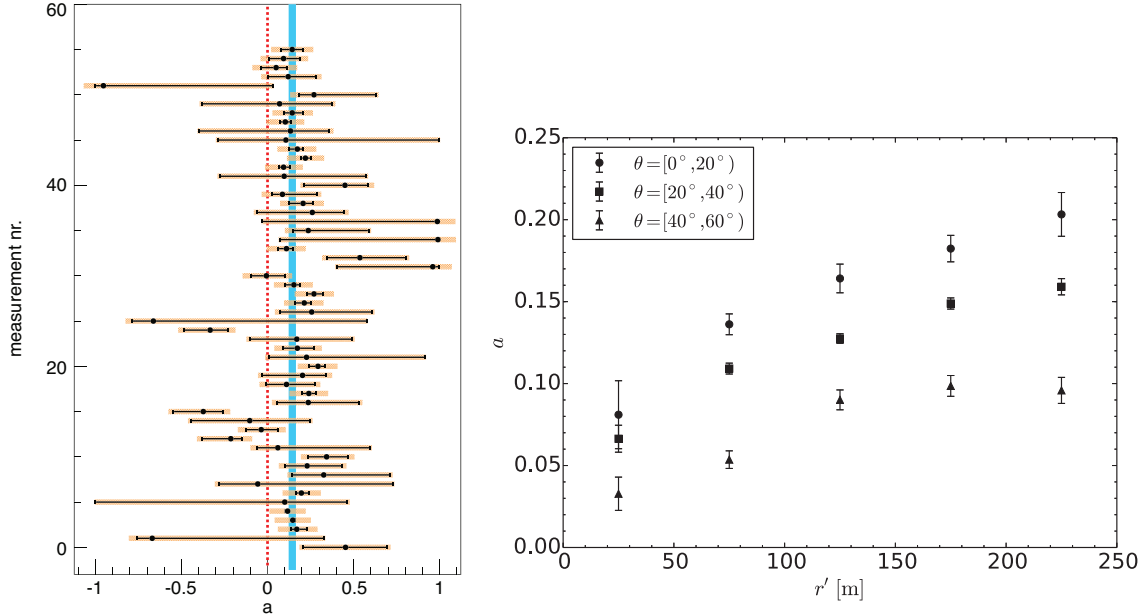


**Fig. 4.** Radio emission processes in the atmosphere. The ratio  $a$  between contributions due to the Askaryan effect and the geomagnetic emission is plotted as measured at the Auger Observatory for different air showers (*left*) [29] and as a function of the distance to the shower axis (in the shower plane) for showers with different zenith angles as measured by LOFAR (*right*) [30].

[30]. The figure illustrates that the contribution through the Askaryan effect increases with increasing distance to the shower axis and it is more pronounced for vertical showers (with small zenith angle).

**Confirmation of simulation codes** The detailed investigations of the properties of the radio emission and the comparison between measurements and predictions from simulations demonstrate that the simulation code CoREAS [31] fully describes all relevant features of the radio emission in air showers and the predictions can be used to interpret the measured air-shower data.

**Probing atmospheric electric fields during thunderstorms** Radio detection of air showers can also be used for auxiliary science, such as the measurements of electric fields in the atmosphere during thunderstorms [32–34]. The footprint of the radio emission from an air shower, which developed during a thunderstorm is shown in Fig. 6 (*right*) [34]. The intensity and polarization patterns of such air showers are radically different from those measured during fair-weather conditions. The figure illustrates the polarization as measured with individual LOFAR antennas (arrows) in the shower plane. An arrow labeled "normal" indicates the expected polarization direction for fair-weather conditions. LOFAR antennas are grouped into circular stations, of which seven are depicted. The position of the shower axis, orthogonal to the shower plane, is indicated by the intersection of the dashed lines. With the use of a simple two-layer model for the atmospheric electric field, these patterns can be well reproduced by state-of-the-art simulation codes. This in turn provides a novel way to study atmospheric electric fields.

#### 4. Measuring properties of cosmic rays with the radio technique

The ultimate objective is to fully characterize the incoming cosmic ray with the radio measurements, i.e., to determine its arrival direction, its energy, and the particle type/mass (see, e.g., [35]).

**Arrival direction** A precise description of the shape of the shower front is essential to correctly reconstruct the direction of the incoming cosmic ray. Different shapes have been investigated at LO-

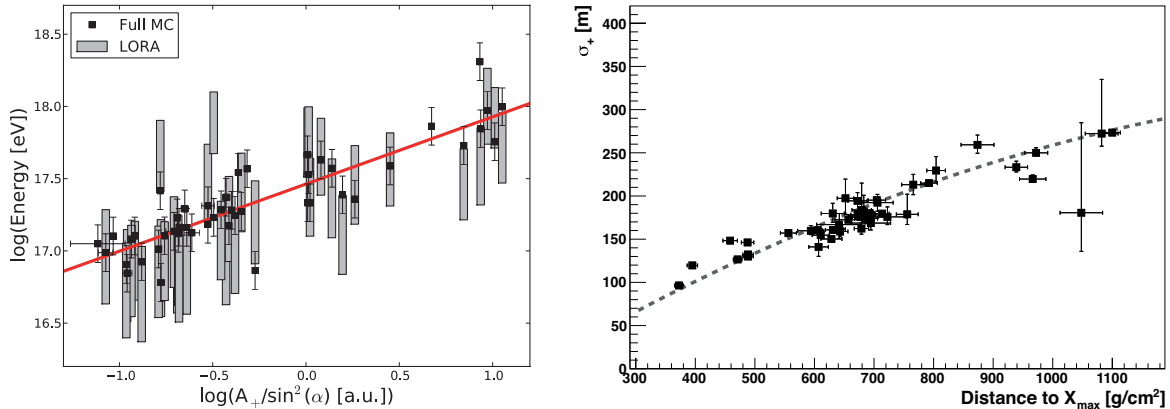


**Fig. 5.** Determining the properties of cosmic rays with radio measurements [22]. *Left:* Energy of the cosmic ray (determined from simulations and measured with the LORA air shower array) as a function of the integrated measured radio power. *Right:* Width of the footprint of the radio emission as a function of the distance to the shower maximum.

FAR as discussed above [20]. Reconstructing the arrival directions of the same measured showers with different wavefront shapes results in differences in the reconstructed arrival directions of typically less than  $1^\circ$  between a plane and a hyperboloid and typically less than  $0.1^\circ$  between a cone and a hyperboloid. Based on these investigations it is expected that the angular resolution for the arrival direction of the shower is better than  $1^\circ$ . Corresponding analyses at the Auger Observatory are under way, expecting a similar precision.

**Energy** The parameters of the function to model the intensity pattern of the radiation on the ground (as described above) are sensitive to the properties of the shower-inducing cosmic rays [22]. The integral of the measured power density is proportional to the shower energy. This is illustrated in Fig. 5 (*left*). The shower energy is plotted as a function of a parameter, that is proportional to the integrated power. The measured signal strength is corrected for a factor, which depends on the angle between the shower axis and the direction of the geomagnetic field. This is necessary, since the dominant geomagnetic emission strongly depends on this angle. The shower energy is determined in two ways in the figure: it is derived from Monte Carlo simulations (using CORSIKA [36] and CoREAS) and it has been measured with the particle detector array at LOFAR (LORA). A clear correlation can be seen between the shower energy and the measured radio intensity on the ground.

A very sophisticated analysis is ongoing at the Auger Observatory [37–39]. The energy content of the radio emission in air showers in the frequency range 30 – 80 MHz has been measured on an absolute scale. A 1 EeV air shower, arriving perpendicularly to the geomagnetic field radiates 15.8 MeV in the radio frequency regime. Since radio emission is not suffering from attenuation in the atmosphere and the radiation strength can be calculated from first principles, measuring the radio emission seems to be a very promising tool to establish the absolute energy scale of air-shower detectors.

**Depth of the shower maximum** Several methods are studied at LOFAR and the Auger Observatory to derive the type of the incoming cosmic ray or its atomic mass  $A$  from the radio measurements. The key is to measure the depth of the shower maximum in the atmosphere, which is proportional to  $\ln A$ . The width of the measured footprint is proportional to the geometrical distance from the antennas to the position of the shower maximum. This correlation is shown in Fig. 5 (*right*). This method is used at LOFAR and at the Auger Observatory to estimate the cosmic-ray mass [19, 22].

To obtain a precise value of the depth of the shower maximum for each shower, we apply the following procedure, originally developed at LOFAR and now also applied at the Auger Observatory [19, 40]. The shower direction and energy are obtained from the measured signals in the particle de-

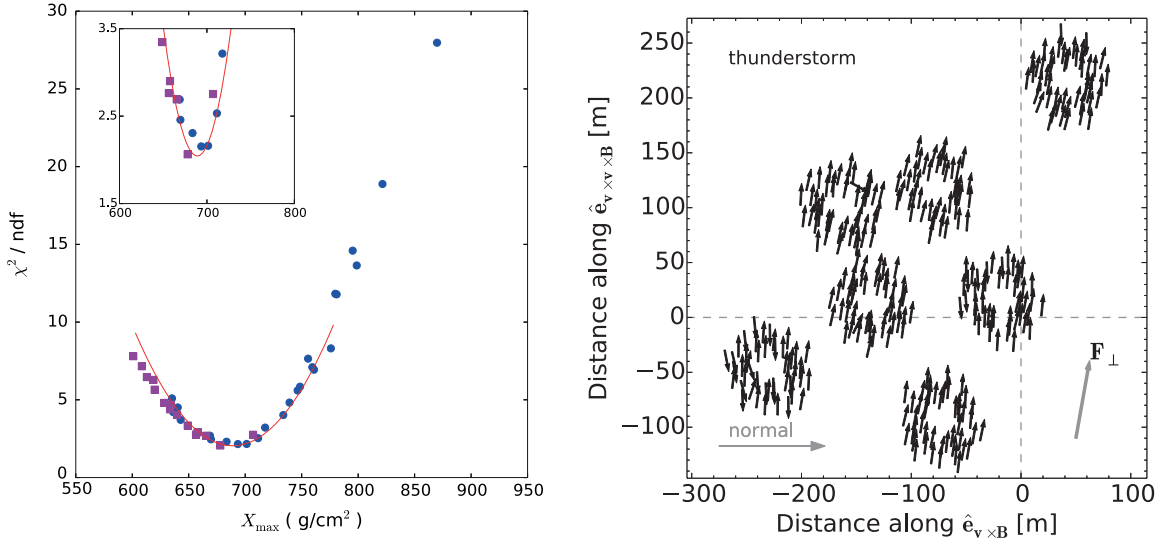


**Fig. 6.** *Left:* Determining the depth of the shower maximum from the radio measurements. The  $\chi^2$  values of simulated showers are shown as a function of the depth of the shower maximum [40]. *Right:* Footprint of the radio emission of an air shower, which developed during a thunderstorm [34].

tectors and the radio antennas. With these parameters simulations are initiated, simulating the development of air showers and the accompanying radio emission, using the CORSIKA and the CoREAS codes, for primary protons and iron nuclei. Due to fluctuations in the individual particle interactions in an air shower this results in cascades with a wide distribution for the depth of the shower maximum (all of them having the same energy and direction of incidence as the measured one). The predicted signals in the particle detectors and the radio antennas are then compared to the measurements. A  $\chi^2$  method is used to determine the simulated shower which best matches the measured values. This yields a value for the depth of the shower maximum. The method is illustrated in Fig. 6 (*left*). The  $\chi^2$  values are depicted as a function of the depth of the shower maximum  $X_{\text{max}}$ . A parabola is fitted to the  $\chi^2$  values and the minimum of this function gives the estimated  $X_{\text{max}}$  value for the measured shower. With this method  $X_{\text{max}}$  is determined with an accuracy of  $17 \text{ g/cm}^2$  at LOFAR. At the Auger Observatory this method is used to compare the depth of the shower maximum as obtained from the radio measurements with the  $X_{\text{max}}$  values measured with the fluorescence detectors. Quantitative analyses of the achieved accuracy are under way.

At the Auger Observatory other mass-sensitive observables are also investigated: the shape of the shower front is sensitive to the geometrical distance to the shower maximum; the shape of the shower front is approximated with a hyperboloid and the angle between the shower plane and the hyperboloid (at large distances from the shower axis) is sensitive to  $X_{\text{max}}$ . The spectral shape of the measured radio signal is also sensitive to  $X_{\text{max}}$  [41]. This could be a very promising method for a sparse radio array, where the only measurable radio signals are detected in a small number of radio detectors.

## References

- [1] J. Blümer, R. Engel, J. Hörandel, Prog. Part. Nucl. Phys. 63 (2009) 293.
- [2] M. Nagano, A. Watson, Rev. Mod. Phys. 72 (2000) 689.
- [3] H. Falcke, P. Gorham, Astropart. Phys. 19 (2003) 477.
- [4] H. Falcke, et al., Nature 435 (2005) 313.
- [5] D. Ardouin, et al., Nucl. Instr. Meth. A 555 (2005) 148.
- [6] D. Kostunin, et al., Nucl. Instrum. Meth. A 742 (2014) 89.

- [7] T. Huege, *Braz. J. Phys.* 44 (2014) 520.
- [8] M. van Haarlem, et al., *Astron. Astrophys.* 556 (2013) A2.
- [9] P. Schellart, et al., *Astron. Astrophys.* 560 (2013) A98.
- [10] S. Thoudam, et al., *Nucl. Instrum. Meth.* A767 (2014) 339.
- [11] S. Thoudam, et al., *Astropart. Phys.* 73 (2015) 34
- [12] J. Abraham, et al., *Nucl. Instr. Meth. A* 523 (2004) 50.
- [13] J. Abraham, et al., *Nucl. Instrum. Meth. A* 620 (2010) 227.
- [14] A. Aab, et al., *Nucl. Instr. Meth. A* 798 (2015) 172.
- [15] C. Meurer, N. Scharf, *Astrophys. Space Sci. Trans.* 7 (2011) 183.
- [16] D. Charrier, *Nucl. Instrum. Meth. A* 662 (2012) S142.
- [17] P. Abreu, et al., *JINST* 7 (2012) P10011.
- [18] P. Abreu, et al., *Nucl. Instrum. Meth. A* 635 (2011) 92.
- [19] J. Schulz, et al., *Proceedings 34th International Cosmic Ray Conference, Den Haag (2015), Proceedings of Science (ICRC2015)* 615.
- [20] A. Corstanje, et al., *Astropart. Phys.* 61 (2015) 22.
- [21] A. Nelles, et al., *Astropart. Phys.* 60 (2015) 13.
- [22] A. Nelles, et al., *JCAP* 1505 (05) (2015) 018.
- [23] H. Allan, *Progress in Elementary Particles and Cosmic Ray Physics*, J.G. Wilson and S.G. Wouthuysen eds., North Holland, 1971, p. 169.
- [24] A. Nelles, et al., *Astropart. Phys.* 65 (2014) 11.
- [25] W. Apel, et al., *JCAP* 1409 (09) (2014) 025.
- [26] D. Ardouin, et al., *Astropart. Phys.* 31 (2009) 192.
- [27] V. Marin, *Proceedings, 32nd International Cosmic Ray Conference, Beijing, 1* (2011) 291.
- [28] A. Bellétoile, et al., *Astropart. Phys.* 69 (2015) 50.
- [29] A. Aab, et al., *Phys. Rev. D* 89 (5) (2014) 052002.
- [30] P. Schellart, et al., *JCAP* 1410 (10) (2014) 014.
- [31] T. Huege, M. Ludwig, C. W. James, *ARENA 2012, AIP Conf. Proc.* 1535 (2013) 128.
- [32] S. Buitink, et al., *Astron. Astroph.* 467 (2007) 385.
- [33] W. Apel, et al., *Adv. Space Res.* 48 (2011) 1295.
- [34] P. Schellart, et al., *Phys. Rev. Lett.* 114 (16) (2015) 165001.
- [35] W. D. Apel, et al., *Phys. Rev. D* 90 (6) (2014) 062001.
- [36] D. Heck, et al., *Report FZKA 6019, Forschungszentrum Karlsruhe* (1998).
- [37] C. Glaser, et al., *AIP Conf. Proc.* 1535 (2013) 68.
- [38] C. Glaser, et al., *Proceedings 34th International Cosmic Ray Conference, Den Haag (2015), Proceedings of Science (ICRC2015)* 364.
- [39] A. Aab, et al., Submitted to: *Phys. Rev. D* (arXiv 1508.04267).
- [40] S. Buitink, et al., *Phys. Rev. D* 90 (8) (2014) 082003.
- [41] S. Grebe, et al., *AIP Conf. Proc., 5th Int. ARENA Workshop 2012* 1535 (2013) 73.